

WeatherDiffusion: Weather-Guided Diffusion Model for Forward and Inverse Rendering

YIXIN ZHU, Nanjing University, China
 ZUOLIANG ZHU, Nankai University, China
 MILOŠ HAŠAN, Adobe Research, NVIDIA Research, USA
 JIAN YANG, Nanjing University, China
 JIN XIE*, Nanjing University, China
 BEIBEI WANG*, Nanjing University, China

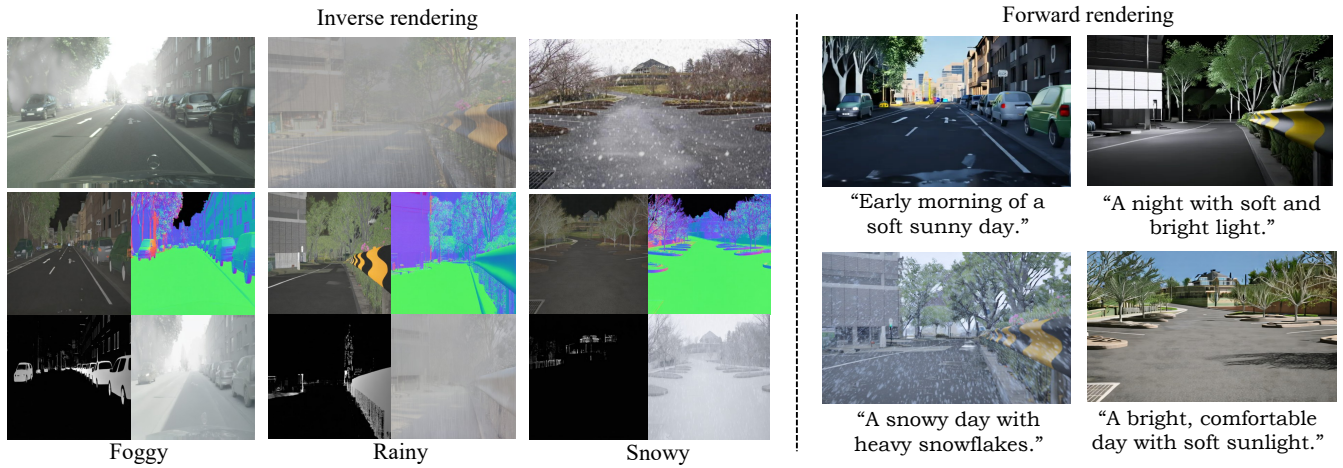


Fig. 1. By leveraging a latent diffusion model, combined with explicit visual guidance based on intrinsic maps, our method achieves high-quality results in both forward and inverse rendering. Here, we show three real-world inputs under different weather conditions. The left part illustrates the inverse rendering results, while the right part shows forward rendering with modified weather and lighting based on the intrinsic maps.

Forward and inverse rendering have emerged as key techniques for enabling understanding and reconstruction in the context of autonomous driving (AD). However, complex weather and illumination pose great challenges to this task. The emergence of large diffusion models has shown promise in achieving reasonable results through learning from 2D priors, but these models are difficult to control and lack robustness. In this paper, we introduce WeatherDiffusion, a diffusion-based framework for forward and inverse rendering on AD scenes with various weather and lighting conditions. Our method enables authentic estimation of material properties, scene geometry, and lighting, and further supports controllable weather and illumination editing through the use of predicted intrinsic maps guided by text descriptions. We observe that different intrinsic maps should correspond to different regions of the original image. Based on this observation, we propose Intrinsic map-aware attention (MAA) to enable high-quality inverse rendering. Additionally, we introduce a synthetic dataset (i. e. WeatherSynthetic) and a real-world dataset (i. e. WeatherReal) for forward and inverse rendering on AD scenes with diverse weather and lighting. Extensive experiments show that our WeatherDiffusion outperforms state-of-the-art methods on

several benchmarks. Moreover, our method demonstrates significant value in downstream tasks for AD, enhancing the robustness of object detection and image segmentation in challenging weather scenarios.

CCS Concepts: • **Computing methodologies** → *Rendering*.

Additional Key Words and Phrases: Diffusion models, Inverse rendering, Rendering

1 INTRODUCTION

Forward and inverse rendering lie at the heart of scene understanding in autonomous driving (AD). Forward rendering (FR) generates photo-realistic images under various lighting and weather conditions, assisting learning-based models in gaining comprehensive knowledge of scenes. Inverse rendering (IR) aims to recover the underlying scene properties—such as geometry, material, and lighting—from observed images, enabling more controllable and flexible applications (e.g., material editing, relighting, and augmented reality). However, both tasks encounter difficulties in the complex AD scenarios. Traditional FR methods (e.g., rasterization and ray tracing) rely on reasonable and detailed inputs that are difficult to obtain in real-world autonomous driving scenarios. Meanwhile, IR

*Corresponding author.

Authors' addresses: Yixin Zhu, Nanjing University, China, yixinzhu@smail.nju.edu.cn; Zuoliang Zhu, Nankai University, China, nkuzhuzl@gmail.com; Miloš Hašan, Adobe Research, NVIDIA Research, USA, mihasan@adobe.com; Jian Yang, Nanjing University, China, csjyang@njust.edu.cn; Jin Xie, Nanjing University, China, csjxie@nju.edu.cn; Beibei Wang, Nanjing University, China, beibei.wang@nju.edu.cn.

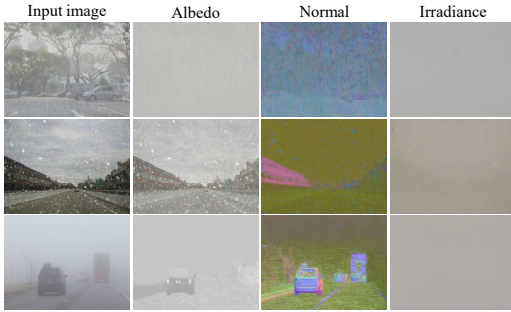


Fig. 2. Existing methods struggle to process different weather. The first column shows input images with rain, snow, and fog, sampled from TransWeather [Valanarasu et al. 2021] and DAWN [Kenk and Hassaballah 2020]. The following columns present the inverse rendering results of $RGB \leftrightarrow X$ [Zeng et al. 2024].

is a typical ill-posed problem. Without extra priors, multiple plausible decompositions exist for the same image, making reasonable decompositions challenging.

Recent advances in diffusion models [Esser et al. 2024; Ho et al. 2020; Ramesh et al. 2022] have shown promise in addressing such problems through probabilistic modeling and conditional generation. Existing approaches [Kocsis et al. 2024; Li et al. 2024; Liang et al. 2025; Zeng et al. 2024] have achieved impressive results at the indoor and object levels, successfully decoupling lighting and material properties and providing reasonable estimations. However, existing methods do not yet support a FR and IR framework for large-scale, multi-weather autonomous driving scenarios. As shown in Fig. 2, current state-of-the-art methods struggle to provide reasonable estimation under various weather conditions.

The AD scenes present unique challenges compared with indoor scenes or object-level tasks. First, complex and dynamic weather conditions, along with diverse natural illumination, complicate the FR and IR. Rain, fog, and snow drastically change the lighting conditions, occlude geometric cues, and influence surface characteristics by specular reflections and occlusions. Meanwhile, poor weather conditions reduce the visibility and make distant features almost imperceptible in the scene. Second, unlike indoor scenes where object scale is limited by the confined space and maximum room depth, AD scenes exhibit much larger variations in object scale due to the open and extended layout of roads. This introduces challenges for both dataset generalization and the model’s attention mechanisms. Without task-specific guidance, the model may waste capacity on irrelevant regions or fail to capture subtle details necessary for reasonable decomposition. Last, the absence of a large-scale, high-quality dataset presents a significant challenge for this task.

To address these challenges, we propose: (1) **Weather-guided diffusion** trained on new datasets specifically constructed for AD scenes under diverse weather and lighting conditions. We choose Stable Diffusion 3.5 medium¹ (SD 3.5) as base model because it can generate images that match textual conditions well. We fine-tune it to better support forward and inverse rendering tasks. To

enhance the robustness of our model under various weather conditions, we construct a synthetic and a real-world dataset designed for large-scale AD scenes. (2) **Intrinsic map-aware attention (MAA)** that enables the model to focus on critical local regions based on spatial and structural characteristics, inspired by the observation that different intrinsic maps naturally attend to different local regions (e.g., metallicity often corresponds to cars and poles, normal is associated with surfaces like roads and buildings). This module increases weights of patches according to characteristics of different maps. It extracts a set of high-level semantic vectors based on these patches and feeds them into the diffusion model as visual guidance. Our framework decomposes an image into several maps in IR. In FR, our framework synthesizes images based on intrinsic maps under different lighting and weather conditions prompted by text. By proactively correcting environmental distortions at the visual input level, we significantly boost the performance of downstream tasks such as object detection and semantic segmentation.

In conclusion, our main contributions are summarized as follows:

- We construct WeatherDiffusion, a framework to decompose images into intrinsic maps under various weather conditions, and synthesize them into another lighting or weather condition guided by text prompts.
- We devise MAA that provides customized visual detail guidance for generative models, helping our model to decompose reasonable maps.
- We construct two new datasets called WeatherSynthetic and WeatherReal, containing synthetic and real-world images covering various weather conditions on autonomous driving scenarios, along with their corresponding maps.

2 RELATED WORK

Generative model. Generative model aims to learn the underlying distribution of data and generate new samples that align with the true data. With the rapid development of deep learning, plenty of works have emerged to generate high-quality results using text or image as the condition. VAE [Kingma et al. 2013] leverages variational inference for probabilistic modeling, enabling explicit likelihood estimation but often producing blurry samples. GAN [Goodfellow et al. 2014] employs adversarial training to generate sharp, high-fidelity outputs, yet suffers from mode collapse and unstable optimization. More recently, diffusion models [Esser et al. 2024; Ho et al. 2020; Ramesh et al. 2022; Rombach et al. 2022] have demonstrated the capability to generate high-fidelity, text-aligned, and stylistically diverse images. Diffusion models such as Stable diffusion [Esser et al. 2024; Rombach et al. 2022] and DALL-E [Ramesh et al. 2022] mostly follow DDPM [Ho et al. 2020] and its enhancements [Lipman et al. 2022; Liu et al. 2022; Song et al. 2020], which divide the generation process into two distinct phases: forward process and reverse process. In the forward process, the original image is gradually corrupted by adding Gaussian noise until it converges to a Gaussian distribution. The reverse process employs a neural network, including UNet [Ronneberger et al. 2015] and DiT [Peebles and Xie 2023], to iteratively denoise samples drawn from this Gaussian distribution, ultimately reconstructing the target image.

¹<https://huggingface.co/stabilityai/stable-diffusion-3.5-medium>

In our research, we utilize diffusion models to estimate material, geometry, and lighting from a single image of the AD scene. We fine-tune SD 3.5 on our datasets. By injecting additional prior conditions into the diffusion model, we demonstrate that leveraging the prior knowledge embedded in pre-trained diffusion models enables the recovery of clean textures, intricate geometric details, and plausible lighting information.

Inverse rendering. IR aims to recover scene-level physical properties such as geometry, material, and lighting from observed images. Intrinsic image decomposition is a common formulation of IR, and our method focuses on it, so we mainly review intrinsic image decomposition in this paragraph. Recent intrinsic image decomposition methods [Janner et al. 2017; Yu and Smith 2019; Zhu et al. 2022] often used a learning-based framework on large-scale dataset [Li et al. 2020; Roberts et al. 2021; Zhu et al. 2022]. These deep learning-driven approaches have enabled intrinsic image decomposition models to surpass the limitations of Lambertian reflectance assumptions, achieving predictive capacities for physically based rendering (PBR)-oriented material properties, geometric structures, and illumination parameters.

Forward and inverse rendering using diffusion. The emergence of latent diffusion model has catalyzed a novel methodology that leverages generative model to learn the joint probability distribution between images and their corresponding intrinsic maps [Chen et al. 2024; Fu et al. 2024; Kocsis et al. 2024; Li et al. 2024; Liang et al. 2025; Zeng et al. 2024]. IID [Kocsis et al. 2024] firstly train a latent diffusion model to estimate material, including albedo, roughness and metallicity. RGB \leftrightarrow X [Zeng et al. 2024] propose a framework using diffusion models for both FR and IR. DiffusionRenderer [Liang et al. 2025] finetunes Stable Video Diffusion [Blattmann et al. 2023] to maintain temporally consistent estimation. However, prevailing methods are predominantly designed for indoor scenes or object-level tasks, whereas AD environments exhibit dynamic and intricate illumination conditions coupled with expanded scene dimensions. Current approaches struggle to adequately process such vehicular scenarios solely through the inherent generalization capabilities of generative models. In parallel, the presence of different weather (e.g., rain, snow, fog) in driving environments induces substantial performance degradation in existing systems. To address these challenges, we devise extra priors for diffusion models to empower enhanced decomposition of AD scenes into constituent intrinsic layers.

3 BACKGROUND

In this section, we briefly introduce forward and inverse rendering. Then, we discuss a crucial assumption to apply the IR diffusion to autonomous driving scenes. Finally, we present basic concepts of the diffusion model.

3.1 Forward and inverse rendering

Forward rendering. In conventional FR pipelines, pixel colors are computed by solving the rendering equation, which needs precise knowledge of geometry, material, and lighting. However, acquiring such comprehensive information is typically infeasible in the wild

(e.g., AD scenes). Recently, the emergence of the diffusion model has brought another way to render a scene, without precise scene knowledge. Specifically, the diffusion model renders images based on decomposed intrinsic maps predicted from inverse-rendering methods and a lighting condition prompted by text, which can be formulated as:

$$I \sim p_\theta(I|\{\mathbf{a}, \mathbf{n}, \mathbf{r}, \mathbf{m}, \mathbf{i}\}, \mathbf{p}), \quad (1)$$

where I denotes the rendered image, $\{\mathbf{a}, \mathbf{n}, \mathbf{r}, \mathbf{m}, \mathbf{i}\}$ is the set of intrinsics, and \mathbf{p} is the text prompt indicating the weather condition.

Inverse rendering. IR aims to decompose geometry, material, and lighting from a single or multiple image(s). A widely adopted setting [Zeng et al. 2024] is to decompose an image into these components described by intrinsic maps, known as intrinsic image decomposition. Specifically, the material is represented by albedo map $\mathbf{a} \in \mathbb{R}^{W \times H \times 3}$, roughness map $\mathbf{r} \in \mathbb{R}^{W \times H}$ and metallicity map $\mathbf{m} \in \mathbb{R}^{W \times H}$ defined in Principled bidirectional reflectance distribution function [Burley and Studios 2012]. The geometry is described by the normal map $\mathbf{n} \in \mathbb{R}^{W \times H \times 3}$, and the lighting condition is defined by the irradiance map $\mathbf{i} \in \mathbb{R}^{W \times H \times 3}$. These intrinsics can be formulated as a conditional probability distribution:

$$X_i \sim q_\theta(X_i|I, \mathbf{p}^c), \quad (2)$$

where X_i denotes the target intrinsic, q_θ represents a distribution parameterized by θ , I is the input image and \mathbf{p}^c is the textual condition indicating the intrinsic to decompose. In practice, a prevailing solution is to use a generative model (e.g., diffusion model) to approximate this q_θ .

Discussion. Although some weather-related phenomena encountered in AD scenes—such as raindrops, fog, and dust—have complex models in reality, we assume these phenomena are primarily reflected in the irradiance component, while material properties (e.g., albedo) remain unaffected. We find that this simple assumption is sufficient to handle our task in most scenes.

3.2 Diffusion model

Given image $I \in \mathbb{R}^{H \times W \times 3}$ and intrinsic map $\mathbf{y} \in \mathbb{R}^{H \times W \times C}$, diffusion model employs a pre-trained encoder to map them from pixel space to a latent space and then get the latent variable:

$$\mathbf{x}_0 = \mathcal{E}(I), \quad \mathbf{z}_0 = \mathcal{E}(\mathbf{y}). \quad (3)$$

Compared to previous versions, SD 3.5 redesigns the latent space to have 16 channels instead of 4, which proves beneficial for handling outdoor scenes characterized by larger view ranges and more complex scale variations. Following Rectified Flow Matching [Lipman et al. 2022], a random noise is added to latent component:

$$\mathbf{z}_t = (1-t)\mathbf{z}_0 + t\epsilon, \quad \epsilon \sim \mathcal{N}(\mathbf{0}, \mathbf{I}), \quad (4)$$

where t represents denoising timestep and ϵ is random noise sampled from a Gaussian distribution. Then DiT [Peebles and Xie 2023] is used to estimate the velocity field at a specific timestep. The estimation can be mathematically expressed as:

$$\mathbf{v}_\theta(\mathbf{z}_t, \mathbf{c}, t) = \frac{d\mathbf{z}_t}{dt} = \epsilon - \mathbf{z}_0, \quad (5)$$

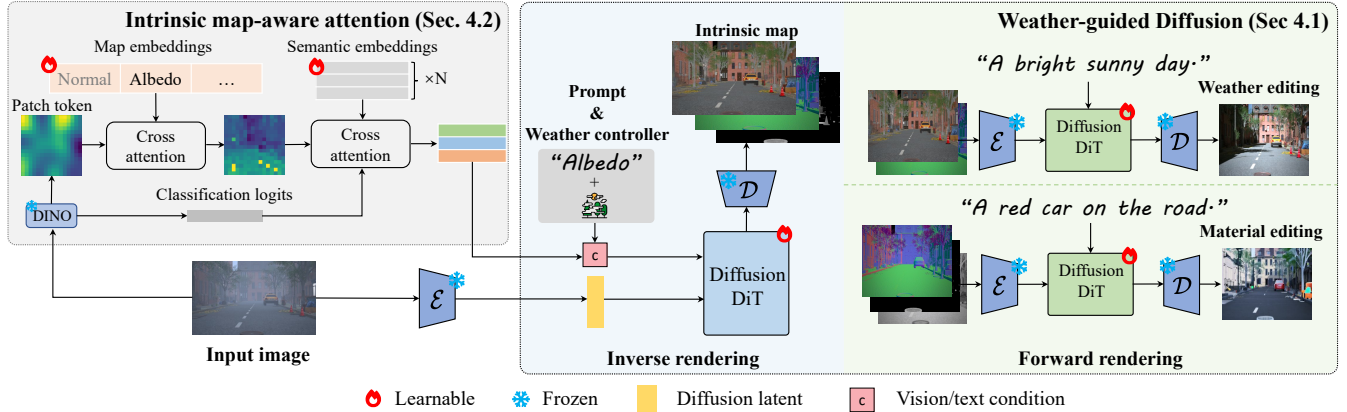


Fig. 3. An overview of our method. We propose a weather-guided diffusion for FR and IR. The IR diffusion decomposes images into intrinsic maps, including a weather controller that discriminates similar weather. We further design Intrinsic map-aware attention to extract important tokens corresponding to target intrinsic maps, where the learned map and semantic embeddings filter patch tokens via attentions. These filtered tokens serve as the visual condition for the IR diffusion. On the other hand, the FR diffusion renders images based on given decomposed maps and text prompts that specify the target condition, which preserves intrinsic attributes while modifying the weather or materials.

where c is the vision or text condition. This is achieved by minimizing the following loss function:

$$L_\theta = \mathbb{E}_{t \sim \mathcal{U}(0,1), \epsilon \sim \mathcal{N}(0,1)} [\|v_\theta(z_t, c, t) - (\epsilon - z_0)\|_2^2]. \quad (6)$$

Once the velocity field is estimated, the noisy latent variable is progressively denoised step by step, resulting in a clean estimation of the original latent variable.

4 METHOD

In this section, we present our weather-guided diffusion for forward and inverse rendering of AD scenes under various weather conditions first (Sec. 4.1) and then design Intrinsic Map-Aware Attention (MAA) that provides semantic guidance for IR (Sec. 4.2).

4.1 Weather-guided diffusion

We finetune two separate SD 3.5, enabling IR and FR, respectively. The IR diffusion performs intrinsic decomposition, disentangling images into material, geometry, and illumination. Correspondingly, the FR one renders images based on given intrinsic maps and text prompts that specify the target weather condition or material.

Inverse rendering. We observe that the original SD 3.5 struggles to distinguish low-visibility weather conditions and shadowed regions, as they are similar in insufficient lighting. Hence, the model tends to generate rain or snow textures in shadowed regions.

To address this issue, we categorize weather conditions into nine classes based on similarities in lighting and particle types (e.g., rain-drop and snowflake), including “sunny”, “rainy/thunderstorm”, “snow”, “foggy” and others. These categories are encoded as one-hot vectors, named the weather controller. Following GeoWizard [Fu et al. 2024], we apply positional encoding to the controller first and then add up the encoded controller, the timestep vector, and text projection to obtain the diffusion condition. This condition is passed through an MLP to predict the scale and shift parameters for a LayerNorm (LN)

and applied to the input features as:

$$\{\alpha, \beta\} = \text{MLP}(f_{\text{weather}}(r_i) + f_{\text{time}}(t) + f_{\text{text}}(\tau(c))), \quad (7)$$

$$h_{\text{norm}} = \text{LN}(h) \odot (1 + \alpha) + \beta, \quad (8)$$

where r_i is the positional-encoded weather controller, $t \sim \mathcal{U}(0, T)$ is denoising timestep, $\tau(c)$ is projection of text prompt. These three conditions are summed and passed through an MLP to produce the scaling and shifting coefficients α, β for the hidden states h , where \odot represents element-wise product.

Forward rendering. The FR diffusion conditions on the decomposed maps and specified weather conditions prompted by text to render images. To enhance the model’s robustness to absent intrinsic maps, we randomly drop a subset of them during training following $\text{RGB} \leftrightarrow X$ [Zeng et al. 2024]. In such cases, the missing maps are replaced with zero matrices:

$$M = \{\hat{z}_a, \hat{z}_n, \hat{z}_r, \hat{z}_m, \hat{z}_i\}, \quad \hat{z}_i = \begin{cases} 0, & \text{w.p. } p \\ z_i, & \text{w.p. } 1 - p \end{cases}. \quad (9)$$

where z_i is the latent map calculated following Eqn.(3), p is the probability of dropping the map.

4.2 Intrinsic map-aware attention

Since IR relies heavily on capturing the structural and intrinsic properties of the image, textual guidance of original SD 3.5 is unsuitable for this task. To this end, we explore replacing the textual guidance with visual priors to capture the structural and semantic information required by the decomposition. We observe that different intrinsic maps require attention to distinct regions of an image. For instance, albedo prediction demands a focus on fine-grained object textures, whereas normal estimation primarily concerns the overall orientation of large surfaces such as the ground and walls. Metallic prediction, in contrast, needs to selectively attend to metallic objects such as vehicles, poles, and railings. Meanwhile, we notice that the

patch tokens extracted by DINO [Oquab et al. 2023] exhibit strong intra-class consistency, meaning that spatially separated regions corresponding to the same type of material or structure produce highly similar feature representations. To leverage these observations, we devise Intrinsic map-aware attention (MAA) to extract detailed visual guidance for diffusion.

First, we explore how to filter important regions according to intrinsic maps. Then, we extract semantic embeddings from these regions. Specifically, we first employ DINOv2 [Oquab et al. 2023] to extract a set of patch tokens \mathbf{p} , where each token encodes the features of a specific spatial region. For each intrinsic map, we define a set of learnable embeddings $\mathbf{d} \in \mathbb{R}^{D_{\text{model}}}$ that capture its inherent characteristics. A gating mechanism with map-aware attention is then applied to filter the patch tokens according to the current intrinsic map, producing map-aware patch tokens that emphasize regions relevant to the target map:

$$\mathbf{p}' = \text{gating}(\mathbf{p}, \mathbf{d}) = \text{Softmax}\left(\frac{(\mathbf{d}\mathbf{W}_Q)(\mathbf{p}\mathbf{W}_K)^T}{\sqrt{d_k}}\right)\mathbf{p}\mathbf{W}_V, \quad (10)$$

where \mathbf{p}' is map-aware patch tokens calculated by map-aware attention, which applies cross-attention between map embedding \mathbf{d} and patch tokens \mathbf{p} . We show attention score heatmap in Fig. 4.

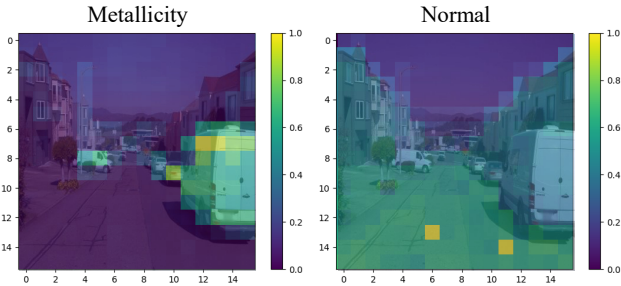


Fig. 4. Intrinsic map-aware attention visualization. We reveal the heatmaps of attention probability of metallicity (left) and normal (right). Intrinsic map-aware attention can assign higher weights to the corresponding regions of the intrinsic map.

Instead of using these patch tokens directly, we introduce a set of learnable embeddings, corresponding to semantic categories. The embeddings are first modulated by the classification logits from DINO. These modulated features are fused with the map-aware patch tokens via a cross-attention mechanism. The aggregated representation is then combined with the map embeddings to construct the final visual condition input to the DiT model:

$$\mathbf{c}' = \alpha \cdot \text{Softmax}\left(\frac{(\mathbf{c}\mathbf{W}_Q)(\mathbf{p}'\mathbf{W}_K)^T}{\sqrt{d_k}}\right)\mathbf{p}'\mathbf{W}_V + \mathbf{c}, \quad (11)$$

where α is a learnable coefficient, \mathbf{c} is learnable semantic embeddings, \mathbf{p}' is map-aware tokens calculated following Eqn. (10).

5 DATASET CONSTRUCTION

The existing datasets suffer from the absence of outdoor environments (OpenRooms [Li et al. 2020], Hypersim [Roberts et al. 2021],

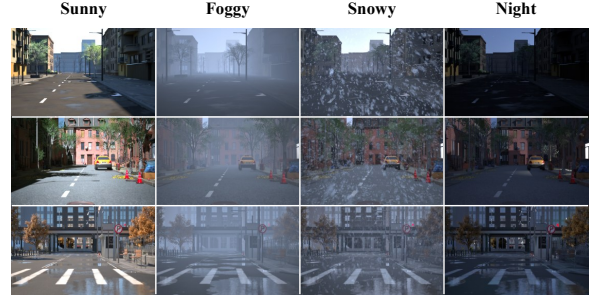


Fig. 5. Example of our WeatherSynthetic. Each row shows a scene rendered under diverse lighting and weather conditions.

InteriorVerse [Zhu et al. 2022]) or the insufficiency of weather diversity (MatrixCity [Li et al. 2023]), thus inappropriate for large-scale AD scenes under complex weather conditions. Therefore, we propose WeatherSynthetic and WeatherReal, including various weather types and rich corresponding intrinsic maps. The overview of these datasets is shown in Tab. 1.

WeatherSynthetic. We construct WeatherSynthetic: a large-scale synthetic dataset encompassing a wide range of scene types and weather conditions:

- **Weather types:** sunny, overcast, rainy, thunderstorm, snowy, foggy, sandstorm.
- **Times of day:** early morning, morning, noon, afternoon, night.
- **Environments:** urban, suburban, highway, parking

We use Unreal Engine 5² to render all images and intrinsic maps. We purchase 3D assets that are allowed to be used in generative models³ in Fab. The rendering pipeline includes a movie render queue and multi-sample anti-aliasing, promising high-quality images and intrinsic maps. The UltraDynamicSky and UltraDynamicWeather are applied to modify the weather and daytime. Note that all images are in linear space without tone mapping. This way, we get 35K images at the cost of 24h. Some typical scenes are shown in Fig. 5.

WeatherReal. Additionally, we propose WeatherReal: a real-world dataset for IR on AD scenes with various weather conditions. We apply weather augmentation on open-source datasets such as Waymo [Sun et al. 2020] and Kitti [Geiger et al. 2013]. Since these datasets were collected under sunny conditions, the model trained on WeatherSynthetic is adequate for generating pseudo ground truth. Our data augmentation strategy integrates generative models with image processing techniques. Specifically, we first employ a pre-trained image editing model (i. e. InstructPix2Pix [Brooks et al. 2023]) to alter the ground and objects within the scene, such as converting dry surfaces to wet ones or covering clean objects with snow. Additionally, leveraging the provided depth maps, we synthesize realistic fog effects and simulate falling snowflakes or raindrops using randomized noise patterns. Our WeatherReal is motivated by the observation

²<https://www.unrealengine.com>

³<https://www.fab.com/eula>

Table 1. Comparison of our datasets and previous datasets for IR. Our dataset includes both synthetic and real-world data, and simulates a wide variety of weather and lighting conditions. Meanwhile, we provide detailed map annotations for each scene. Each feature is marked as satisfied (✓), partially satisfied (✓), or not satisfied (✗).

	Images	Scene	Source	Weather	Intrinsic map				
					Albedo	Normal	Roughness	Metallicity	Irradiance
InteriorVerse	50K	Indoor	Synthetic	✗	✓	✓	✓	✓	✗
Hypersim	70K	Indoor	Synthetic	✗	✓	✓	✗	✗	✓
Openrooms	118K	Indoor	Synthetic	✗	✓	✓	✓	✗	✗
Matrixcity	316K	City	Synthetic	✓	✓	✓	✓	✓	✗
WeatherSynthetic	35K	City	Synthetic	✓	✓	✓	✓	✓	✓
WeatherReal	10K	City	Real-world	✓	✓	✓	✓	✓	✓

Table 2. Quantitative evaluations of our method against existing methods in terms of decomposition quality on the WeatherSynthetic test set. Considering that IID and RGB↔X were only trained on indoor datasets, we finetune them on our WeatherSynthetic and show the results before and after finetuning. We highlight the best results in red and the second-best ones in orange.

Method	Albedo			Normal			Roughness		Metallic		Irradiance	
	PSNR↑	SSIM↑	LPIPS↓	PSNR↑	SSIM↑	MAE↓	PSNR↑	LPIPS↓	PSNR↑	LPIPS↓	PSNR↑	LPIPS↓
IID	7.80	0.26	0.63	–	–	–	10.30	0.55	12.37	0.64	–	–
IID (w/ finetune)	11.55	0.53	0.40	–	–	–	12.34	0.43	12.22	0.55	–	–
RGB↔X	9.66	0.44	0.47	11.90	0.41	15.51	13.62	0.55	–	–	16.24	0.58
RGB↔X (w/ finetune)	11.35	0.59	0.37	16.14	0.49	7.05	13.65	0.57	11.96	0.66	16.38	0.69
GeoWizard	–	–	–	16.24	0.54	12.47	–	–	–	–	–	–
IDArb	6.40	0.48	0.65	10.77	0.43	22.42	10.70	0.62	14.66	0.62	–	–
ours	18.02	0.66	0.35	20.95	0.61	4.24	15.03	0.45	18.94	0.14	23.55	0.29
ours (w/o MAA)	17.35	0.66	0.45	18.82	0.49	5.56	13.96	0.51	18.04	0.28	23.41	0.43

that after training our model merely on synthetic data, its performance degrades on some real-world samples with extreme weather conditions. This is mainly due to the domain gap between synthetic and real-world data, as well as the severe degradation caused by extreme weather conditions in real-world data, such as heavy fog and torrential rain.

6 EXPERIMENT RESULTS

In this section, we present the evaluation setups first. Then, we conduct comparisons and ablation studies on the AD datasets. Eventually, we discuss our limitations. We present our training and inference details in the supplementary material.

6.1 Metrics and baselines

Following previous works [Li et al. 2024; Zeng et al. 2024], we use Peak Signal-to-Noise Ratio (PSNR), Structural Similarity Index Measure (SSIM), Mean Angular Error (MAE), and Learned Perceptual Image Patch Similarity (LPIPS) to evaluate inverse rendering results. We choose RGB↔X [Zeng et al. 2024], IID [Kocsis et al. 2024], GeoWizard [Fu et al. 2024] and IDArb [Li et al. 2024] for comparisons. Note that IID and RGB↔X are trained on the indoor dataset, GeoWizard is trained across indoor and outdoor scenes, and IDArb is limited to the object level. Although our method is primarily

designed for AD scenarios, it also achieves state-of-the-art performance on indoor benchmarks. We show quantitative and qualitative results in the supplementary material.

6.2 Inverse rendering

In this subsection, we first conduct quantitative evaluations on WeatherSynthetic, then we evaluate on real-world datasets including WeatherReal, Waymo [Sun et al. 2020], DAWN [Kenk and Hassaballah 2020], and TransWeather [Valanarasu et al. 2021].

Synthetic data. We show the comparison between our method and existing methods on the test set of our WeatherSynthetic in Tab. 2. We achieve state-of-the-art on all metrics. We finetune IID [Kocsis et al. 2024] and RGB↔X [Zeng et al. 2024] with the same training steps on our WeatherSynthetic. Their performance improves, but they fail to provide high-quality estimation. Qualitative results are shown in Fig. 8. We compare our WeatherDiffusion with other methods under different weather conditions. In albedo estimation (Fig. 8a), our method effectively recovers fine details of the albedo while completely separating illumination from material. Although RGB↔X removes lighting effects, it lacks accuracy. IID and IDArb mistakenly interpret shadows as albedo. After fine-tuning, their

accuracy improves, but they fail to recover details. In normal estimation (Fig. 8b), particles in the air, such as snowflakes, can severely obscure geometric details. Our model successfully eliminates the impact of snowflakes and restores clean and sharp normals. Other methods are significantly affected. In roughness and metallicity estimation (Fig. 8c–Fig. 8d), due to blurring, faithfully estimating the roughness and metallicity of vehicles hidden in rain and fog is extremely challenging. Our model successfully detects distant vehicles, while all other methods fail. The fine-tuned RGB \leftrightarrow X and IID perform comparably to our method in roughness estimation, but still fail to precisely distinguish between metallic and non-metallic objects. In contrast to albedo estimation, irradiance estimation (Fig. 8e) aims to recover lighting conditions. We selected a sunny day with large shadows to showcase the results, where RGB \leftrightarrow X performs as well as our model. On the other hand, our WeatherDiffusion successfully captures the presence of rain while maintaining clear details of distant vehicles and buildings. Full comparison and more results are shown in the supplementary material.

Real data. We show a comparison of real images with various weather in Fig. 10. The first image is from Waymo [Sun et al. 2020], and our WeatherDiffusion provides reasonable estimation for all intrinsic maps. This demonstrates that our model generalizes well from synthetic data to real-world data. Fine-tuned RGB \leftrightarrow X gives decent albedo and normal estimation, but fails on vehicles and distant buildings. IDArb struggles to decouple shadow and material on albedo, while failing to provide reasonable roughness and metallicity estimation. The other three images show different weather conditions (such as raindrops on the lens, heavy rain, and dense fog), where our WeatherDiffusion provides reasonable estimations. They are both sampled from TransWeather [Valanarasu et al. 2021] dataset. We will show more results in the supplementary material.

6.3 Forward rendering

Synthetic data. We show a comparison of forward rendering between WeatherDiffusion and RGB \leftrightarrow X in Fig. 9. We use albedo and normal as input, and use “A sunny day in the city” as the text prompt. Our WeatherDiffusion recovers material and geometry better than RGB \leftrightarrow X, which tends to generate abnormal textures of the road and buildings. Moreover, our WeatherDiffusion generates images that align well with the text descriptions.

Real data. As shown in Fig. 11 and Fig. 12, our WeatherDiffusion leverages intrinsic maps obtained in inverse rendering to generate re-rendered images with different weather and lighting conditions according to text prompts. In the first line of Fig. 11, we use albedo and normal as input, and our WeatherDiffusion can generate image that closely matches the material and geometry of the original image. At the second line, we use normal, roughness, and metallicity as input. Our WeatherDiffusion change materials and weather conditions according to the prompt at the same time. We show more qualitative results in the supplementary material.

6.4 Ablation Study

Effect of MAA. As highlighted in Sec. 4, a key observation of our method is that different intrinsic maps should pay attention to

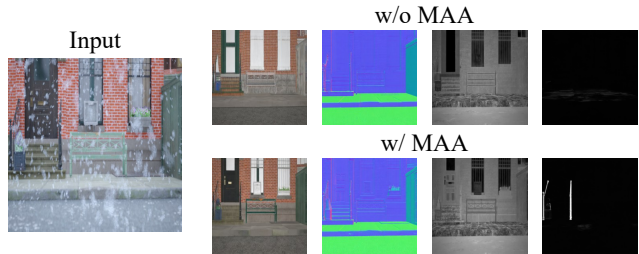


Fig. 6. Ablation study on MAA.

different regions of the image. Our MAA provides such guidance for diffusion to help improve the quality of inverse rendering. We train an IR diffusion model without MAA, replacing the visual condition with original text guidance. As shown in Tab. 2, for both indoor scene and AD scene, the model without MAA behaves poorly than our full model. We show a qualitative result in Fig. 6. With the semantic guidance related to the map provided by MAA, the model produced more refined geometry and material predictions and successfully identified the metallic handrail, assigning it a reasonable level of metallicity.

Effect of WeatherSynthetic and WeatherReal. We explore the effect of our two datasets separately. We train the IR diffusion model with only the indoor dataset and only the synthetic dataset. The qualitative results are shown in the supplementary material.

6.5 Discussion and limitations

Despite the strong generalization ability of our model on real-world data, we observe some typical scenarios where the model struggles to generalize well. First, our model struggles to estimate out-of-distribution objects such as cranes and heavy trucks that never appear in the training set. Second, in heavy fog conditions, where distant regions are completely occluded, the model has difficulty distinguishing between sky and buildings, often resulting in abnormal albedo and normal predictions. We show a typical failure case in Fig. 7, and more failure cases are shown in the supplementary material.

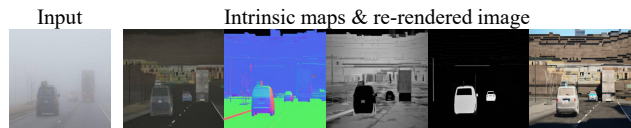


Fig. 7. A typical failure case on a foggy scene. WeatherDiffusion fails to discriminate between the sky and the building hiding behind fog.

7 APPLICATIONS

In AD scenes, object detection and image segmentation are crucial for understanding the environment. Although existing methods [Carion et al. 2020; Xie et al. 2021] have achieved high accuracy, adverse weather conditions can significantly degrade their performance. Our approach decomposes the scene into physical attributes and renders images under new weather and lighting conditions, providing clean inputs for detection and segmentation models. As

shown in Fig. 12, segmentation and detection models struggle to produce reasonable predictions on the original image due to severe occlusions. Our re-rendered image completely removes the snowflakes while strictly preserving the original objects' positions and shapes, enabling the models to generate accurate predictions.

8 CONCLUSION

We propose WeatherDiffusion, a novel framework capable of forward and inverse rendering in AD scenes. It achieves decent intrinsic decomposition across diverse weather and illumination conditions and enables high-quality, editable image generation based on maps and prompt. We propose MAA to provide detailed visual cues to help the model focus on semantically important regions. Last, we construct two datasets, WeatherSynthetic and WeatherReal, offering photorealistic images with intrinsic maps to address the lack of large-scale AD rendering datasets under varied conditions.

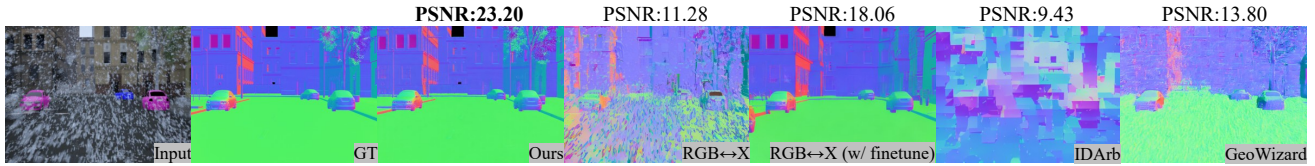
Future directions include reducing dependence on high-quality training data. Combining diffusion models with reinforcement learning—guided by human or LLM feedback—could enhance robustness. Moreover, the emergence of auto-regressive generative models presents opportunities to further advance both rendering and inverse rendering tasks.

REFERENCES

- Andreas Blattmann, Tim Dockhorn, Sumith Kulal, Daniel Mendelevitch, Maciej Kilian, Dominik Lorenz, Yam Levi, Zion English, Vikram Voleti, Adam Letts, et al. 2023. Stable video diffusion: Scaling latent video diffusion models to large datasets. *arXiv preprint arXiv:2311.15127* (2023).
- Tim Brooks, Aleksander Holynski, and Alexei A Efros. 2023. Instructpix2pix: Learning to follow image editing instructions. In *Proceedings of the IEEE/CVF conference on computer vision and pattern recognition*. 18392–18402.
- Brent Burley and Walt Disney Animation Studios. 2012. Physically-based shading at disney. In *Acm Siggraph*, Vol. 2012. vol. 2012, 1–7.
- Nicolas Carion, Francisco Massa, Gabriel Synnaeve, Nicolas Usunier, Alexander Kirillov, and Sergey Zagoruyko. 2020. End-to-end object detection with transformers. In *European conference on computer vision*. Springer, 213–229.
- Zhifei Chen, Tianshuo Xu, Wenheng Ge, Leyi Wu, Dongyu Yan, Jing He, Luozhou Wang, Lu Zeng, Shunsi Zhang, and Yingcong Chen. 2024. Uni-Renderer: Unifying Rendering and Inverse Rendering Via Dual Stream Diffusion. *arXiv preprint arXiv:2412.15050* (2024).
- Patrick Esser, Sumith Kulal, Andreas Blattmann, Rahim Entezari, Jonas Müller, Harry Saini, Yam Levi, Dominik Lorenz, Axel Sauer, Frederic Boesel, et al. 2024. Scaling rectified flow transformers for high-resolution image synthesis. In *Forty-first international conference on machine learning*.
- Xiao Fu, Wei Yin, Mu Hu, Kaixuan Wang, Yuexin Ma, Ping Tan, Shaojie Shen, Dahua Lin, and Xiaoxiao Long. 2024. Geowizard: Unleashing the diffusion priors for 3d geometry estimation from a single image. In *European Conference on Computer Vision*. Springer, 241–258.
- Andreas Geiger, Philip Lenz, Christoph Stiller, and Raquel Urtasun. 2013. Vision meets robotics: The kitti dataset. *The international journal of robotics research* 32, 11 (2013), 1231–1237.
- Ian J Goodfellow, Jean Pouget-Abadie, Mehdi Mirza, Bing Xu, David Warde-Farley, Sherjil Ozair, Aaron Courville, and Yoshua Bengio. 2014. Generative adversarial nets. *Advances in neural information processing systems* 27 (2014).
- Jonathan Ho, Ajay Jain, and Pieter Abbeel. 2020. Denoising diffusion probabilistic models. *Advances in neural information processing systems* 33 (2020), 6840–6851.
- Michael Jamner, Jiajun Wu, Tejas D Kulkarni, Ilker Yildirim, and Josh Tenenbaum. 2017. Self-supervised intrinsic image decomposition. *Advances in neural information processing systems* 30 (2017).
- Mourad A Kenk and Mahmoud Hassaballah. 2020. DAWN: vehicle detection in adverse weather nature dataset. *arXiv preprint arXiv:2008.05402* (2020).
- Diederik P Kingma, Max Welling, et al. 2013. Auto-encoding variational bayes.
- Peter Kocsis, Vincent Sitzmann, and Matthias Nießner. 2024. Intrinsic image diffusion for indoor single-view material estimation. In *Proceedings of the IEEE/CVF Conference on Computer Vision and Pattern Recognition*. 5198–5208.
- Yixuan Li, Lihan Jiang, Linning Xu, Yuanbo Xiangli, Zhenzhi Wang, Dahua Lin, and Bo Dai. 2023. Matrixcity: A large-scale city dataset for city-scale neural rendering and beyond. In *Proceedings of the IEEE/CVF International Conference on Computer Vision*. 3205–3215.
- Zhengqin Li, Mohammad Shafiei, Ravi Ramamoorthi, Kalyan Sunkavalli, and Manmohan Chandraker. 2020. Inverse rendering for complex indoor scenes: Shape, spatially-varying lighting and svbrdf from a single image. In *Proceedings of the IEEE/CVF conference on computer vision and pattern recognition*. 2475–2484.
- Zhibing Li, Tong Wu, Jing Tan, Mengchen Zhang, Jiaqi Wang, and Dahua Lin. 2024. IDArb: Intrinsic Decomposition for Arbitrary Number of Input Views and Illuminations. *arXiv preprint arXiv:2412.12083* (2024).
- Ruofan Liang, Zan Gojcic, Huan Ling, Jacob Munkberg, Jon Hasselgren, Zhi-Hao Lin, Jun Gao, Alexander Keller, Nandita Vijaykumar, Sanja Fidler, et al. 2025. Diffusion-Renderer: Neural Inverse and Forward Rendering with Video Diffusion Models. *arXiv preprint arXiv:2501.18590* (2025).
- Yaron Lipman, Ricky TQ Chen, Heli Ben-Hamu, Maximilian Nickel, and Matt Le. 2022. Flow matching for generative modeling. *arXiv preprint arXiv:2210.02747* (2022).
- Luping Liu, Yi Ren, Zhijie Lin, and Zhou Zhao. 2022. Pseudo numerical methods for diffusion models on manifolds. *arXiv preprint arXiv:2202.09778* (2022).
- Maxime Oquab, Timothée Darcet, Théo Moutakanni, Huy Vo, Marc Szafraniec, Vasil Khalidov, Pierre Fernandez, Daniel Haziza, Francisco Massa, Alaaeldin El-Nouby, et al. 2023. Dinov2: Learning robust visual features without supervision. *arXiv preprint arXiv:2304.07193* (2023).
- William Peebles and Saining Xie. 2023. Scalable diffusion models with transformers. In *Proceedings of the IEEE/CVF international conference on computer vision*. 4195–4205.
- Aditya Ramesh, Prafulla Dhariwal, Alex Nichol, Casey Chu, and Mark Chen. 2022. Hierarchical text-conditional image generation with clip latents. *arXiv preprint arXiv:2204.06125* 1, 2 (2022), 3.
- Mike Roberts, Jason Ramapuram, Anurag Ranjan, Atulit Kumar, Miguel Angel Bautista, Nathan Paczan, Russ Webb, and Joshua M Susskind. 2021. Hypersim: A photorealistic synthetic dataset for holistic indoor scene understanding. In *Proceedings of the IEEE/CVF international conference on computer vision*. 10912–10922.
- Robin Rombach, Andreas Blattmann, Dominik Lorenz, Patrick Esser, and Björn Ommer. 2022. High-resolution image synthesis with latent diffusion models. In *Proceedings of the IEEE/CVF conference on computer vision and pattern recognition*. 10684–10695.
- Olaf Ronneberger, Philipp Fischer, and Thomas Brox. 2015. U-net: Convolutional networks for biomedical image segmentation. In *Medical image computing and computer-assisted intervention—MICCAI 2015: 18th international conference, Munich, Germany, October 5–9, 2015, proceedings, part III* 18. Springer, 234–241.
- Jiaming Song, Chenlin Meng, and Stefano Ermon. 2020. Denoising diffusion implicit models. *arXiv preprint arXiv:2010.02502* (2020).
- Pei Sun, Henrik Kretschmar, Xerxes Dotiwalla, Aurelien Chouard, Vijaysai Patnaik, Paul Tsui, James Guo, Yin Zhou, Yuning Chai, Benjamin Caine, et al. 2020. Scalability in perception for autonomous driving: Waymo open dataset. In *Proceedings of the IEEE/CVF conference on computer vision and pattern recognition*. 2446–2454.
- Jeya Maria Jose Valanarasu, Rajeev Yasarla, and Vishal M. Patel. 2021. TransWeather: Transformer-based Restoration of Images Degraded by Adverse Weather Conditions. *arXiv:cs.CV/2111.14813*
- Enze Xie, Wenhai Wang, Zhiding Yu, Anima Anandkumar, Jose M Alvarez, and Ping Luo. 2021. SegFormer: Simple and efficient design for semantic segmentation with transformers. *Advances in neural information processing systems* 34 (2021), 12077–12090.
- Ye Yu and William AP Smith. 2019. Inverserendernet: Learning single image inverse rendering. In *Proceedings of the IEEE/CVF Conference on Computer Vision and Pattern Recognition*. 3155–3164.
- Zheng Zeng, Valentin Deschaintre, Iliyan Georgiev, Yannick Hold-Geoffroy, Yiwei Hu, Fujun Luan, Ling-Qi Yan, and Miloš Hašan. 2024. RGB \leftrightarrow X: Image decomposition and synthesis using material- and lighting-aware diffusion models. In *ACM SIGGRAPH 2024 Conference Papers (SIGGRAPH '24)*. Association for Computing Machinery, New York, NY, USA, Article 75, 11 pages. <https://doi.org/10.1145/3641519.3657445>
- Jingsen Zhu, Fujun Luan, Yuchi Huo, Zihao Lin, Zhihua Zhong, Dianbing Xi, Rui Wang, Hujun Bao, Jiayang Zheng, and Rui Tang. 2022. Learning-based inverse rendering of complex indoor scenes with differentiable Monte Carlo raytracing. In *SIGGRAPH Asia 2022 Conference Papers*. 1–8.



(a) **Albedo under sunlight.** The albedo prediction of our WeatherDiffusion remains reliable while effectively eliminating the impact of shadow on material estimation. RGB↔X successfully disentangles shadows from albedo, but the results are inaccurate. IID and IDArb generate a reasonable estimation but fail to remove the shadow completely.



(b) **Normal under snow.** WeatherDiffusion provides constant and sharp normal estimation compared to other methods. Other methods are heavily influenced by snowflake. GeoWizard gives reasonable predictions, but some inaccuracies are observed in fine details, particularly around the edges of vehicles and buildings.



(c) **Roughness under fog.** Our method provides faithful roughness predictions, including for vehicles and buildings obscured by fog. RGB↔X produces overly smooth predictions, resulting in losing details. Both IID and IDArb are severely affected by the presence of fog.



(d) **Metallicity under rain.** Our WeatherDiffusion metallicity estimation is reliable, especially for vehicles, and others fail to notice the vehicle.



(e) **Irradiance under sunlight and rain.** Under sunlight, our WeatherDiffusion recovers the shadow properly. Under rain, we recover the raindrop while maintaining the detail of the lighting.

Fig. 8. Qualitative comparison of inverse rendering on a synthetic autonomous driving scene with various weather. The highest PSNR is marked in bold. We show the full comparison between methods in the supplementary material.

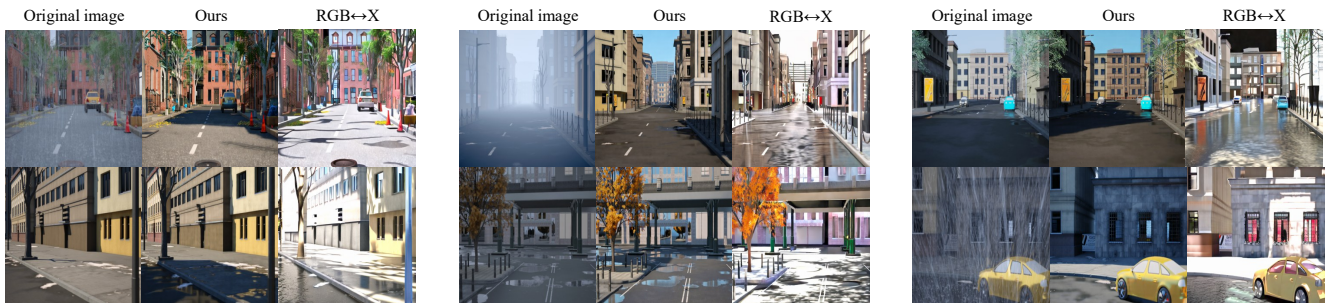


Fig. 9. Comparison of forward rendering results between WeatherDiffusion and RGB↔X on synthetic data.

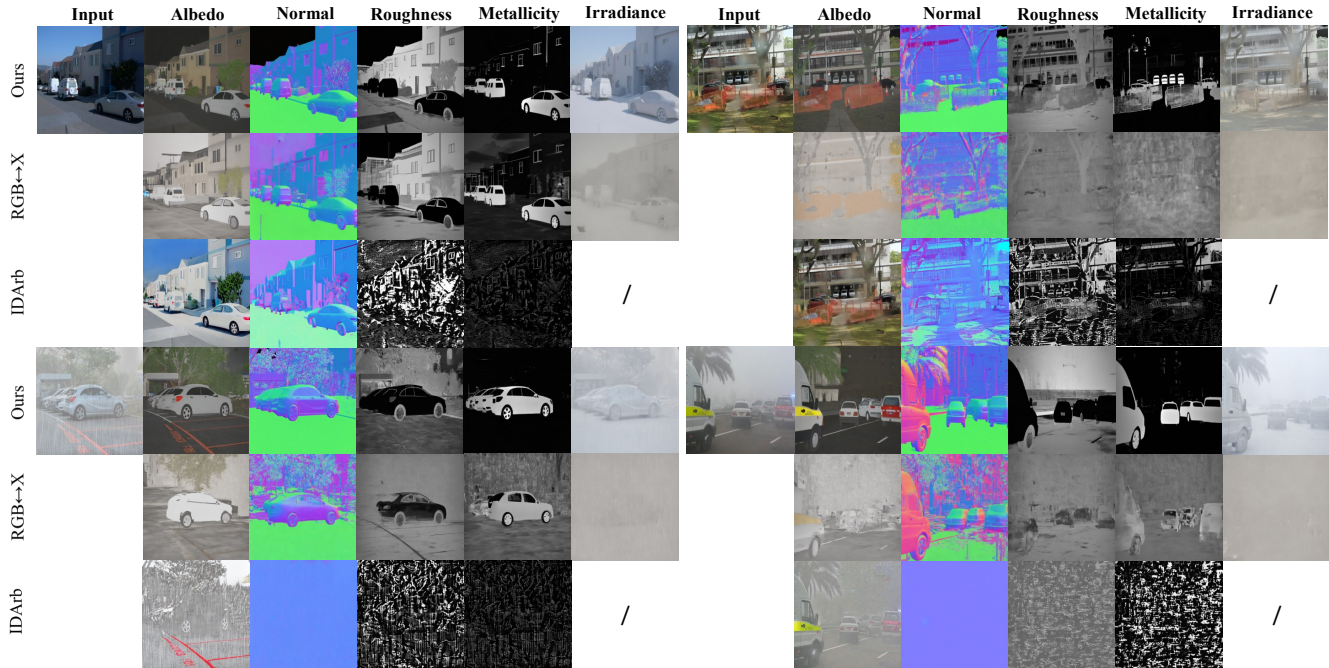


Fig. 10. Comparison of inverse rendering between our method and others on real data with various weather conditions.

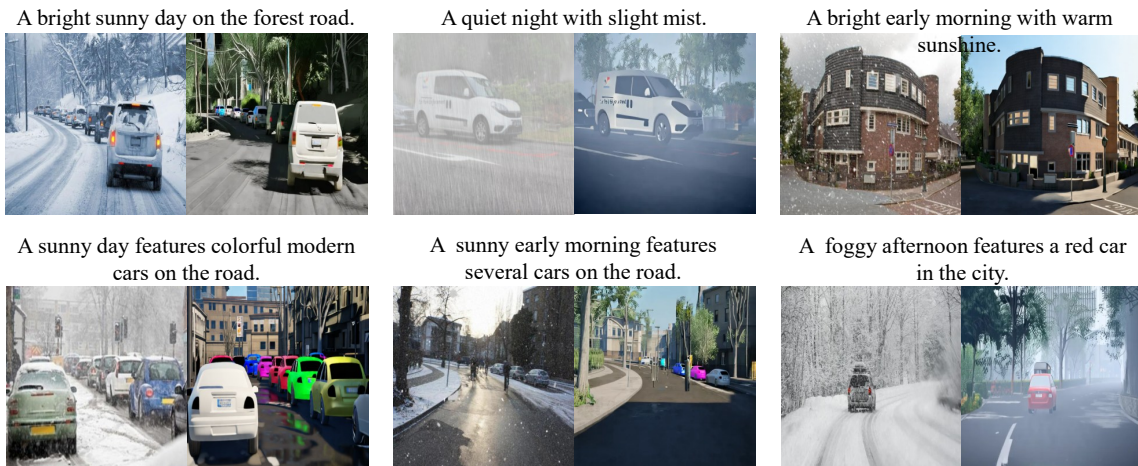


Fig. 11. Forward rendering on real data with different weather conditions. The first image is the original image, and the following is the re-rendered image by our WeatherDiffusion. In the second row, we input normal, roughness, and metallicity, and use a text prompt to edit materials and weather together.



Fig. 12. Our WeatherDiffusion helps the segmentation and detection models improve their performance. Segformer [Xie et al. 2021] and DETR [Carion et al. 2020] fail to give reasonable estimation (e.g., vehicles and buildings) under the heavy snowstorm (left). The first image on the right is the re-rendered image generated by WeatherDiffusion, modifying the weather into sunny. On the re-rendered image, estimations of Segformer and DETR are more reasonable.